

Enhancement of the superconducting transition temperature due to multiband effect in the topological nodal-line semimetal $\text{Pb}_{1-x}\text{Sn}_x\text{TaSe}_2$

K. Kumarasinghe, A. Rahman, M. Tomlinson, and Y. Nakajima*
Department of Physics, University of Central Florida, Orlando, Florida 32816, USA

We report a systematic study of the normal-state and superconducting properties of single crystal $\text{Pb}_{1-x}\text{Sn}_x\text{TaSe}_2$ ($0 \leq x \leq 0.23$). Sn doping enhances the superconducting temperature T_c up to 5.1 K while also significantly increasing impurity scattering in the crystals. For $x = 0$ and 0.018, the specific heat jump at T_c exceeds the Bardeen-Cooper-Schrieffer (BCS) weak-coupling value of 1.43, indicating the realization of strong-coupling superconductivity in undoped and slightly Sn-doped PbTaSe_2 . Substituting Pb with more Sn lowers the specific heat jump at T_c below the BCS value of 1.43, which cannot be explained by a single-gap model. Rather, the observed specific heat data of moderately Sn-doped PbTaSe_2 ($x = 0.08$ and 0.15) are reproduced by a two-gap model. Our observations suggest that additional Fermi pockets appear due to a reduction of the spin-orbit gap with Sn doping, and the multiband effect arising from these emergent Fermi pockets enhances the effective electron-phonon coupling strength, leading to the increase in T_c of $\text{Pb}_{1-x}\text{Sn}_x\text{TaSe}_2$.

I. INTRODUCTION

Noncentrosymmetric superconductors have attracted great interest because of their exotic superconducting properties, including an upper critical field that exceeds the Pauli paramagnetic limit [1, 2] and the realization of unconventional superconductivity [3–5]. The intrinsic lack of the inversion symmetry results in the antisymmetric spin-orbit coupling (SOC) and allows the mixture of spin-singlet (even-parity) and spin-triplet (odd-parity) pairing in the superconducting gap function, even in conventional electron-phonon coupling mechanism. The mixture of the parities can be finely tuned by adjusting the strength of the antisymmetric SOC. Notably, the noncentrosymmetric superconductor $\text{Li}_2(\text{Pd}_{1-x}\text{Pt}_x)_3\text{B}$ exhibits a striking crossover from an even-parity-dominant fully-gapped superconductivity to an odd-parity-dominant nodal superconductivity by controlling Pt concentration [6]. Moreover, noncentrosymmetric superconductors present a promising avenue for realizing topological superconductivity, which can host Majorana-bound states [7].

The topological nodal-line semimetal PbTaSe_2 is one of the intriguing examples of noncentrosymmetric superconductors. Its unique crystal structure—characterized by alternating layers of Pb and TaSe_2 along the c axis—lacks inversion symmetry. This material shows superconductivity at the superconducting transition temperature $T_c = 3.6\text{--}3.8$ K [8–10]. Extensive experimental study, including specific heat [8], thermal conductivity [11], penetration depth [12], and μSR measurements [13], have revealed the fully-gapped superconducting state in PbTaSe_2 . Angular-resolved-photoemission spectroscopy has uncovered bulk nodal lines with non-trivial band topology and fully spin-polarized topological surface states, stemming from the asymmetric SOC

and protected by reflection symmetry [9, 14, 15]. The interplay between the bulk fully-gapped superconductivity and the topological surface state can stabilize topological superconductivity through their proximity effect [16]. In addition, SnTaSe_2 , with a weaker SOC strength than PbTaSe_2 , is also predicted to have topological nodal lines and show superconductivity at $T_c = 5.7$ K [17]. Thus, exploring the evolution of superconducting properties by tuning the SOC strength through substituting Pb with Sn in PbTaSe_2 presents an exciting opportunity to realize an exotic superconducting state.

We here report our findings on the normal-state and superconducting properties of single crystal $\text{Pb}_{1-x}\text{Sn}_x\text{TaSe}_2$. Our results show that Sn doping significantly enhances T_c while introducing notable disorder into the crystals, suggesting the robustness of superconductivity against disorder. We observe a slight increase in the Debye temperature estimated from the resistivity and specific heat as Sn doping levels increase. The specific heat jumps at T_c for $x = 0$ and 0.018 exceed the Bardeen-Cooper-Schrieffer (BCS) weak-coupling value of 1.43, indicating the realization of strong-coupling superconductivity in undoped PbTaSe_2 and slightly Sn-doped PbTaSe_2 . On the other hand, more Sn doping suppresses the specific heat jump at T_c less than the BCS value, which cannot easily be explained by the single-gap model. Instead, our specific heat data for moderately Sn-doped PbTaSe_2 agree with the two-gap model. Our observations suggest that Fermi pockets arise from a reduced spin-orbit gap due to Sn substitution, leading to a multiband superconductivity that enhances T_c .

II. EXPERIMENTAL METHODS

Single crystals of $\text{Pb}_{1-x}\text{Sn}_x\text{TaSe}_2$ were grown using the chemical vapor transport method. Polycrystalline $\text{Pb}_{1-x}\text{Sn}_x\text{TaSe}_2$ was first synthesized by the solid-state reaction. High-purity starting elements of Pb, Ta, and Se with the desired Sn concentration were placed in an

* Corresponding author: Yasuyuki.Nakajima@ucf.edu

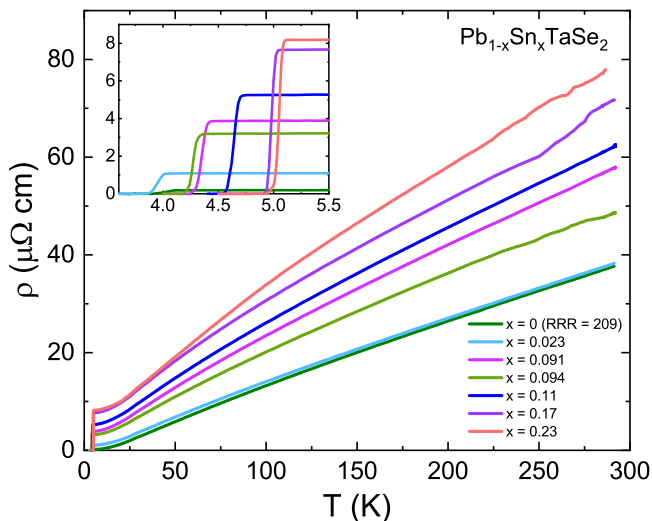


FIG. 1. Overall temperature dependence of the in-plane resistivity of $\text{Pb}_{1-x}\text{Sn}_x\text{TaSe}_2$ at $\mu_0 H = 0$ T. Both undoped and Sn-doped PbTaSe_2 show metallic behavior and undergo a superconducting transition at low temperatures. The inset shows low-temperature resistivity of $\text{Pb}_{1-x}\text{Sn}_x\text{TaSe}_2$.

alumina crucible and sealed inside an evacuated quartz tube. The quartz ampoule was heated at 850°C for 5 days to obtain polycrystals. The obtained polycrystals were ground and placed at one end of a quartz tube along with the transport agent PbCl_2 of 3 mg/cm^3 . The quartz ampoule was then evacuated, sealed, and placed in a two-zone furnace. The hot and cold ends of the furnace were maintained at 850°C and 800°C , respectively, for 3 weeks. Large, shiny, flake-like single crystals were obtained at the cold end.

The crystal structures of the obtained single crystals were characterized using x-ray diffraction. We confirmed the noncentrosymmetric crystal structure of PbTaSe_2 with the space group $P\bar{6}m2$. The Sn concentrations for measured samples were determined using x-ray fluorescence spectroscopy. Specific heat measurements were conducted using the long-relaxation method [18] with a homemade calorimeter.

III. RESULTS AND DISCUSSION

Sn doping enhances T_c of PbTaSe_2 . We present the in-plane resistivity ρ of $\text{Pb}_{1-x}\text{Sn}_x\text{TaSe}_2$ single crystals as a function of temperature (T) in zero magnetic field (FIG.1). For all Sn concentrations x , the resistivity exhibits metallic behavior as the temperature decreases. At high temperatures, the resistivity shows linear-in- T behavior, indicating the dominant electron-phonon scattering.

Regardless of the Sn concentrations, we observe sharp superconducting transitions at low temperatures, as shown in the inset to FIG.1. T_c were determined by the

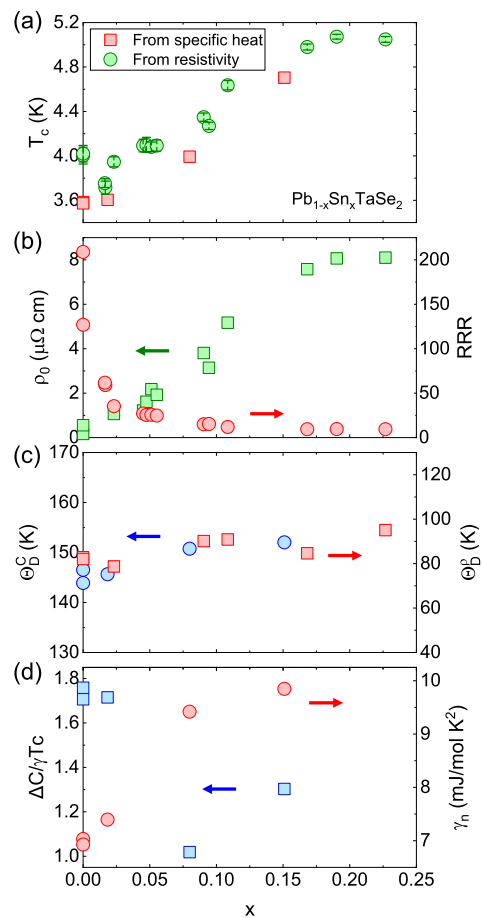


FIG. 2. (a) Superconducting transition temperatures T_c of $\text{Pb}_{1-x}\text{Sn}_x\text{TaSe}_2$ obtained from the resistivity (green circles) and the specific heat (red squares) as a function of Sn concentration x . T_c is defined by the midpoint of resistive transitions and by the local entropy balance in the specific heat measurements. The error bars of T_c obtained from the resistivity represent 10 % and 90 % criteria. (b) The residual resistivity ratio $\text{RRR} = \rho(290\text{K})/\rho(T_c^{\text{onset}})$ (red circles) and the residual resistivity ρ_0 (green squares) versus x . ρ_0 is extracted from a fit to the data below 7 K, using $\rho(T) = \rho_0 + AT^2$. (c) Debye temperature Θ_D^C obtained from the specific heat (blue circles) and Θ_D^ρ obtained from the resistivity (red squares) versus Sn concentration x . Θ_D^C was estimated using $\Theta_D = (12\pi^4 nR/5\beta_{\text{ph}})^{1/3}$ and Θ_D^ρ is extracted from a fit to the resistivity data using the Bloch-Grüneisen formula. (d) Normalized specific heat jump $\Delta C/\gamma_n T_c$ at T_c (blue squares) and the normal-state Sommerfeld coefficient γ_n (red circles) as a function of x . γ_n is extracted from a fit to the data in an applied magnetic field of $\mu_0 H = 1$ T, using $C_n/T = \gamma_n + \beta_{\text{ph}} T^2 + \delta_{\text{ph}} T^4$.

midpoint of the resistive transition. For PbTaSe_2 , superconductivity occurs at $T_c = 4.02$ K, which is slightly higher than the previously reported values of 3.6-3.8 K from the resistivity measurements [8, 15, 19]. We plot T_c obtained from the resistivity measurements as a function of the Sn doping concentration x in FIG.2 (a) (green circles). Notably, T_c increases with Sn doping after show-

ing a slight dip at around $x = 0.03$. Above $x = 0.19$, T_c reaches ~ 5.1 K, by ~ 1.1 K or 26 % higher than the value for $x = 0$.

Sn doping induces disorder in $\text{Pb}_{1-x}\text{Sn}_x\text{TaSe}_2$ while simultaneously increasing T_c . To extract the residual resistivity ρ_0 , we fit the low-temperature resistivity from T_c to 7 K, using $\rho(T) = \rho_0 + AT^2$, where ρ_0 is the residual resistivity and A is a coefficient of electron-electron scattering term. As shown in FIG.2 (b) (green squares), ρ_0 increases from $0.16 \mu\Omega \text{ cm}$ to $8 \mu\Omega \text{ cm}$, a factor of 50, with increasing Sn concentration x . To eliminate uncertainties stemming from geometric factors in calculating the absolute values of the resistivity, we also evaluate the residual resistivity ratio RRR as a scattering measure. The RRR is defined as $\text{RRR} = \rho(290\text{K})/\rho(T_c^{\text{onset}})$ and is plotted as a function of x in FIG.2(b) (red circles). The RRR shows a sharp drop at a slight doping of 2% Sn into PbTaSe_2 and gradually decreases with increasing Sn concentration. The undoped PbTaSe_2 has the largest RRR of 209, while the sample with $x = 0.23$ has the smallest RRR of 9.5, approximately 20 times smaller than that of the undoped sample. Both ρ_0 and RRR indicate that the Sn doping introduces disorders in the system.

To investigate the effect of Sn doping on the electron-phonon coupling, we evaluate the Debye temperature Θ_D . The temperature dependence of the normal-state resistivity due to the electron-phonon scattering can be described by the Bloch–Grüneisen formula,

$$\rho(T) = \rho_0 + A_{\text{BG}} \left(\frac{T}{\Theta_D} \right)^5 \int_0^{\frac{\Theta_D}{T}} \frac{x^5 dx}{(e^x - 1)(1 - e^{-x})}, \quad (1)$$

where A_{BG} is a constant related to the electron-phonon coupling strength [20]. Θ_D , obtained from fits to the resistivity data in the entire temperature range using Eq.(1), is plotted in FIG.2(c) (red squares). For $x = 0$, Θ_D is ~ 83 K, consistent with previously reported values [19, 21]. Θ_D shows weak dependence on x and exhibits a slight increase by 6% at $x = 0.23$, which is qualitatively consistent with substituting heavier Pb with the lighter Sn.

We confirm bulk superconductivity in $\text{Pb}_{1-x}\text{Sn}_x\text{TaSe}_2$ through specific heat measurements. The temperature dependence of the specific heat $C_p(T)$ at 0 T for $\text{Pb}_{1-x}\text{Sn}_x\text{TaSe}_2$ is shown in the inset to FIG.3. In the normal state at high temperatures, the C_p of $\text{Pb}_{1-x}\text{Sn}_x\text{TaSe}_2$ overlap, suggesting that Sn doping has minimal effect on the lattice contribution to the specific heat. Upon lowering temperatures, we observe sharp jumps associated with the superconducting transitions at T_c . T_c was determined using the local entropy balance at the superconducting transition. T_c obtained from the specific heat is plotted as a function of x in FIG.2(a) (green circles). T_c of undoped PbTaSe_2 with $\text{RRR} = 209$ and $\text{RRR} = 127$ are 3.58 K and 3.57 K, respectively. These values are in good agreement with previously reported values obtained from thermodynamic measurements, including specific heat [8] and magnetic susceptibility measurements [22]. However, for undoped

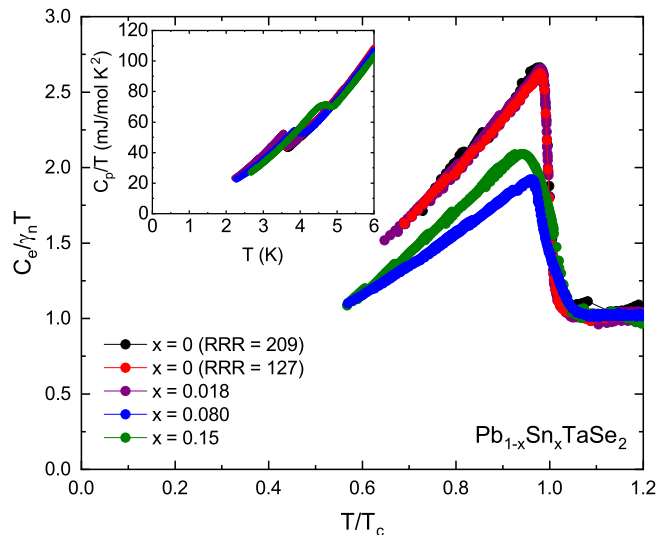


FIG. 3. Normalized electronic specific heat $C_e(T)/\gamma_n T$ of $\text{Pb}_{1-x}\text{Sn}_x\text{TaSe}_2$ as a function of the reduced temperature T/T_c . Inset: temperature dependence of C_p/T of $\text{Pb}_{1-x}\text{Sn}_x\text{TaSe}_2$.

PbTaSe_2 , T_c obtained from the specific heat deviates from those obtained from the resistive transitions. In contrast, at the higher Sn concentrations, T_c obtained from the specific heat are comparable to those obtained from the resistivity measurements.

We take a closer look at the effect of Sn doping on the normal-state specific heat of $\text{Pb}_{1-x}\text{Sn}_x\text{TaSe}_2$. To extract the electronic and lattice contributions to the specific heat, we fit the normal-state specific heat data using the following equation:

$$C_n(T)/T = \gamma_n + C_{\text{ph}}(T)/T, \quad (2)$$

where γ_n is the Sommerfeld coefficient and $C_{\text{ph}}(T) = \beta_{\text{ph}}T^3 + \delta_{\text{ph}}T^5$ represents the phonon contribution to the specific heat, which is assumed to be independent of applied magnetic field. We obtain the normal-state specific heat $C_n(T)$ by applying a magnetic field of 1 T along the c axis, which completely suppresses superconductivity in the measured temperature range for all $\text{Pb}_{1-x}\text{Sn}_x\text{TaSe}_2$. The parameters obtained for PbTaSe_2 with $\text{RRR} = 127$ are $\gamma_n = 6.93 \text{ mJ/mol K}^2$, $\beta_{\text{ph}} = 2.61 \text{ mJ/mol K}^4$, and $\delta_{\text{ph}} = 7.01 \times 10^{-3} \text{ mJ/mol K}^6$, which are in good agreement with previously reported values [8, 10, 19, 21, 23]. As shown in FIG.2(d) (red circles), the obtained γ_n increases with increasing Sn concentration.

The Debye temperature Θ_D is estimated from the extracted β_{ph} using $\Theta_D = (12\pi^4 n R / 5\beta_{\text{ph}})^{1/3}$, where $n = 4$ is the number of atoms per formula unit and $R = 8.314 \text{ J/mol K}$ is the molar gas constant. As plotted in FIG.2(c) (blue circles), the obtained Θ_D is ~ 145 K for $x = 0$ and weakly dependent on x , enhanced only by 3% at $x = 0.15$. Θ_D obtained from the specific heat measurements is about twice as large as that obtained from the resistivity measurements. This discrepancy arises from

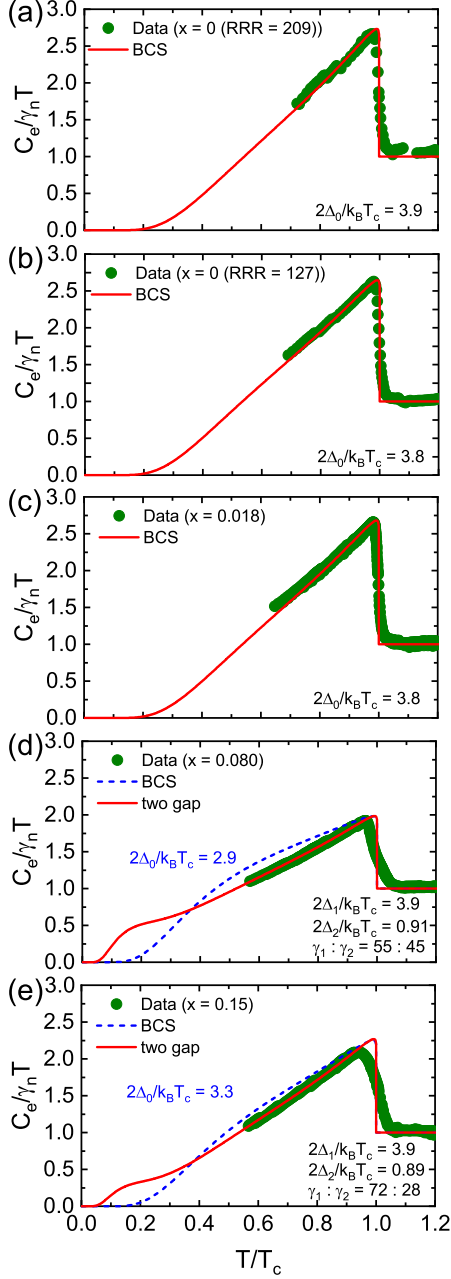


FIG. 4. $C_e(T)/\gamma_n T$ vs T/T_c for (a) $x = 0$ (RRR=209) and (b) $x = 0$ (RRR=127). The red solid curves represent the best fit to each data set using the single-gap model. $C_e(T)/\gamma_n T$ vs T/T_c for (c) $x = 0.018$, (d) $x = 0.080$, and (e) $x = 0.15$. The red solid curves are the best fits to each data set using the two-gap model. The blue-dashed lines are theoretical curves based on the single-gap model, only reproducing the specific heat jump size at T_c .

the different temperature ranges used to estimate Θ_D and has been reported in previous work [19, 21]. Although there is a disparity in the absolute values, both measurements indicate that Θ_D shows only a weak dependence on x .

We now examine the effect of Sn doping on the specific

heat of $\text{Pb}_{1-x}\text{Sn}_x\text{TaSe}_2$ in the superconducting state. The electronic contribution of the specific heat $C_e(T)$ is determined using $C_e(T) = C_p(T) - C_{\text{ph}}(T)$. We plot the normalized electronic specific heat $C_e(T)/\gamma_n T$ versus the normalized temperature T/T_c for different Sn concentrations in the main panel of FIG.3. We observe a sharp jump at T_c for each sample. The normalized values of the specific heat jump $\Delta C/\gamma_n T_c$ at T_c are shown in FIG.2(d) (blue squares). $\Delta C/\gamma_n T_c$ is 1.71 for $x = 0$ (RRR = 127) and 1.76 for $x = 0$ (RRR = 209), both of which are notably larger than the predicted value of 1.43 from the BCS theory for a weak-coupling superconductor. This suggests a possible strong-coupling superconductivity realized in PbTaSe_2 . Our values agree with a previously reported value [8], while other studies have also reported values close to the BCS prediction [10, 19, 23]. Interestingly, while slight Sn doping ($x = 0.018$) does not affect the large specific heat jump at T_c , further Sn doping suppresses $\Delta C/\gamma_n T_c$ less than the predicted value for a weak-coupling superconductor.

To elucidate the superconducting gap amplitude for $\text{Pb}_{1-x}\text{Sn}_x\text{TaSe}_2$, we compare our experimental data with the theoretical calculations based on the α model [24]. In the α model, the entropy S and the specific heat C of the BCS weak-coupling limit can be calculated using the following equations :

$$\frac{S}{\gamma_n T_c} = -\frac{6}{\pi^2} \frac{\Delta_0}{k_B T_c} \int_0^\infty [f \ln f + (1-f) \ln(1-f)] dy, \quad (3)$$

$$\frac{C}{\gamma_n T_c} = t \frac{d(S/\gamma_n T_c)}{dt}, \quad (4)$$

where f is the Fermi-Dirac distribution function defined as $f = [\exp(\beta E) + 1]^{-1}$, $\beta = (k_B T)^{-1}$, and k_B is the Boltzmann constant. The energy of quasiparticle excitations is given by $E = [\epsilon^2 + \Delta^2(t)]^{1/2}$, where ϵ is the energy of the normal electrons relative to the Fermi energy, $t = T/T_c$ is the reduced temperature. The temperature dependence of the energy gap is assumed to be $\Delta(T) = \Delta_0 \tanh 1.82[1.018(T_c/T - 1)]^{0.51}$, where Δ_0 is the gap value at $T = 0$ [25, 26]. The integration variable is $y = \epsilon/\Delta_0$. Set Δ_0 to be a fitting parameter, we fit the normalized electronic specific heat for $x = 0$ to Eq.(4). As shown in FIGs.4(a) and (b), the calculated curves are in excellent agreement with our data for both samples in the measured temperature range. The extracted superconducting gap amplitude, $2\Delta_0/k_B T_c$, is 3.9 for $x = 0$ (RRR = 209) and 3.8 for $x = 0$ (RRR = 127), which are larger than 3.53 predicted for the BCS weak-coupling superconductors, indicating the strong-coupling superconductivity realized in PbTaSe_2 . This strong-coupling superconductivity is insusceptible to slight Sn doping ($x = 0.018$), as shown in FIG.4(c).

However, the single-gap α model cannot reproduce the observed specific heat for moderately Sn-doped PbTaSe_2 . The observed specific heat jumps at T_c for $x = 0.08$ and 0.15 are 1.0 and 1.3, respectively, much smaller than the

BCS weak-coupling limit of 1.43, while the specific heat of slightly Sn-doped PbTaSe₂ ($x = 0.018$) is identical to undoped one, as shown in FIG.3. We calculate the normalized specific heat using the single-gap α model to reproduce the observed small jumps at T_c for $x = 0.08$ and 0.15. This yields the superconducting gap amplitude $2\Delta_0/k_B T_c = 2.9$ for $x = 0.08$ and $2\Delta_0/k_B T_c = 3.3$ for $x = 0.15$, both of which are smaller than the BCS weak-coupling value of 3.53. As shown in FIGs.4(d) and (e), the calculated curves with these small gap amplitudes (blue dashed lines) significantly deviate from the measured data.

The two-gap model proposed for the multigap superconductor MgB₂ explains the observed specific heat for moderately Sn-doped PbTaSe₂ within the measured temperature range [24]. In this model, the specific heat can be expressed as $C = wC_1 + (1 - w)C_2$, where C_1 and C_2 represent the specific heat contribution from band 1 and 2, respectively. These contributions are calculated independently using Eqs.(3) and (4). The relative weights for each band are given by $w = \gamma_1/\gamma_n$ and $1 - w = \gamma_2/\gamma_n$, where γ_i is a partial Sommerfeld constant for band i and $\gamma_n = \gamma_1 + \gamma_2$. As shown in FIG.4 (d) and (e), the theoretical calculations based on the two-gap model are in excellent agreement with our data across the measured temperature range. We obtain the parameters $2\Delta_1/k_B T_c = 3.9$, $2\Delta_2/k_B T_c = 0.91$, and $\gamma_1 : \gamma_2 = 55 : 45$ for $x = 0.080$ and $2\Delta_1/k_B T_c = 3.9$, $2\Delta_2/k_B T_c = 0.89$, and $\gamma_1 : \gamma_2 = 72 : 28$ for $x = 0.15$. The larger gap amplitudes of $x = 0.080$ and 0.15 are very close to those of $x = 0$ and 0.018, and appear to be independent of Sn doping. The smaller gap amplitude of $x = 0.080$ is comparable to that of $x = 0.15$ and seems nearly independent of Sn doping. On the other hand, the ratio of the density of states for bands 1 and 2 varies with Sn doping, which affects the overall shape of the specific heat. Our observations indicate that Sn doping significantly impacts the multigap nature in the superconducting state of Pb_{1-x}Sn_xTaSe₂.

We observe an enhancement of T_c with Sn doping in the noncentrosymmetric superconductor Pb_{1-x}Sn_xTaSe₂, where odd-parity superconducting states are theoretically allowed to exist. This enhancement is seemingly counterintuitive because the impurity scattering due to disorder increases significantly—by a factor of 50, as estimated from ρ_0 and by a factor of 20 from the RRR—and in general, disorder negatively affects the superconductivity. This suggests that superconductivity is strikingly robust against disorders, contrasting with odd-parity superconductivity. The robustness against disorders is further supported by our observations of no discernible effect on the specific heat and T_c in undoped PbTaSe₂ with two different RRR values. These results imply that the contribution from odd-parity pairing in the superconducting gap function is negligible in PbTaSe₂ consistent with previous work reporting the fully-gapped conventional superconducting state [8, 11–13].

Qualitatively, substituting Pb with Sn can enhance T_c due to the lighter atomic mass M of Sn compared to Pb. This substitution slightly increases the Debye temperature ($\propto M^{-1/2}$) as well as the electron-phonon coupling strength λ ($\propto M^{-1}$), leading to an enhancement of T_c , as described by the McMillan formula,

$$T_c = \frac{\Theta_D}{1.45} \exp \left[-\frac{1.04(1 + \lambda)}{\lambda - \mu^*(1 + 0.62\lambda)} \right], \quad (5)$$

where $\mu^* = 0.10 - 0.15$ is the Coulomb repulsive screened parameter [27]. However, the modest increase in Θ_D or λ resulting from $\sim 20\%$ Sn doping is likely too small to account for the enhancement of T_c by more than 40%. The enhancement of effective electron-phonon coupling strength estimated from experimental values using Eq.(5) is discernibly larger than expected solely from the atomic mass contribution. By utilizing $\mu^* = 0.13$, the measured bulk T_c , and Θ_D^C with Eq.(5), we obtain $\lambda = 0.73$ for $x = 0$ and $\lambda = 0.80$ for $x = 0.15$, an increase by $\sim 10\%$. On the other hand, the expected enhancement of λ due to the atomic mass alone can be estimated from the ratio of effective atomic masses [28]:

$$\begin{aligned} \frac{\lambda(\text{Pb}_{1-x}\text{Sn}_x\text{TaSe}_2)}{\lambda(\text{PbTaSe}_2)} &\sim \left[\frac{\Theta_D(\text{Pb}_{1-x}\text{Sn}_x\text{TaSe}_2)}{\Theta_D(\text{PbTaSe}_2)} \right]^2 \\ &= \left[\frac{M_{\text{Pb}}^{3/2} + M_{\text{Ta}}^{3/2} + 2M_{\text{Se}}^{3/2}}{(1-x)M_{\text{Pb}}^{3/2} + xM_{\text{Sn}}^{3/2} + M_{\text{Ta}}^{3/2} + 2M_{\text{Se}}^{3/2}} \right]^{2/3}, \end{aligned} \quad (6)$$

yielding $\lambda(\text{Pb}_{0.85}\text{Sn}_{0.15}\text{TaSe}_2)/\lambda(\text{PbTaSe}_2) = 1.03$. This discrepancy between the observed and expected enhancement of λ indicates additional contributions to λ other than the atomic mass effect.

We attribute this enhancement of the electron-phonon coupling strength to the multiband effect induced by Sn doping, which controls the spin-orbit gap in the band structure of Pb_{1-x}Sn_xTaSe₂. The specific heat data for $x = 0.080$ and 0.15 necessitate the two-gap model to account for the observations, indicating that the multiband effect plays an essential role in the superconducting states of Pb_{1-x}Sn_xTaSe₂. Although the band structures for PbTaSe₂ and SnTaSe₂ are very similar according to ab-initio calculations [17], we speculate that extra Fermi pockets emerge at the Fermi energy, located near the nodal lines around the K and H points in the Brillouin zone, due to a subtle change in the spin-orbit gap size with Sn doping. Indeed, the γ_n is enhanced with Sn concentration x , suggestive of an additional contribution to the density of states from these emergent Fermi pockets compared with the undoped samples. In this scenario, activating the interband coupling between bands enhances the effective electron-phonon coupling constant, inevitably increasing T_c [29], while the larger gap size $2\Delta_1/k_B T_c$ remains unaffected by Sn doping. In addition, the electron-phonon coupling of Pb_{1-x}Sn_xTaSe₂ can be enhanced by the quantum geometric effect due to nontrivial electron band geometry and/or topology

[30]. Indeed, the nontrivial aspect of the band topology of PbTaSe_2 can remain as Sn is substituted for Pb [17]. Further experimental and theoretical efforts are needed to verify this quantum geometric contribution in $\text{Pb}_{1-x}\text{Sn}_x\text{TaSe}_2$.

IV. SUMMARY

In summary, we have measured the resistivity and specific heat of $\text{Pb}_{1-x}\text{Sn}_x\text{TaSe}_2$ single crystals. We observe the enhancement of T_c with the increasing Sn concentration x while also finding a significant increase in impurity scattering with Sn doping, as indicated by the residual resistivity and the residual resistivity ratio. For undoped ($x = 0$) and slightly doped ($x = 0.018$) samples, the spe-

cific heat jump at T_c is greater than the BCS value of 1.43, yet the jump diminishes with Sn doping. The specific heat data of moderately Sn-doped samples are reproduced by theoretical calculations based on the two-gap model, highlighting the pivotal role of emergent Fermi pockets caused by the Sn substitution in the superconducting state. The enhancement of T_c in $\text{Pb}_{1-x}\text{Sn}_x\text{TaSe}_2$ can be attributed to the multiband effect due to these emergent Fermi pockets, driven by a reduction of the spin-orbit coupling via Sn doping.

ACKNOWLEDGMENTS

The authors thank D. Le and V. Turkowski for their valuable discussions. This work was supported by an NSF Career DMR-1944975.

-
- [1] E. Bauer, G. Hilscher, H. Michor, C. Paul, E. W. Scheidt, A. Griбанov, Y. Seropegin, H. Noël, M. Sigrist, and P. Rogl, Heavy Fermion Superconductivity and Magnetic Order in Noncentrosymmetric CePt_3Si , *Phys. Rev. Lett.* **92**, 027003 (2004).
- [2] N. Kimura, K. Ito, H. Aoki, S. Uji, and T. Terashima, Extremely High Upper Critical Magnetic Field of the Noncentrosymmetric Heavy Fermion Superconductor CeRhSi_3 , *Phys. Rev. Lett.* **98**, 197001 (2007).
- [3] H. Q. Yuan, D. F. Agterberg, N. Hayashi, P. Badica, D. Vandervelde, K. Togano, M. Sigrist, and M. B. Salamon, S-Wave Spin-Triplet Order in Superconductors without Inversion Symmetry: $\text{Li}_2\text{Pd}_3\text{B}$ and $\text{Li}_2\text{Pt}_3\text{B}$, *Phys. Rev. Lett.* **97**, 017006 (2006).
- [4] M. Nishiyama, Y. Inada, and G.-q. Zheng, Spin Triplet Superconducting State due to Broken Inversion Symmetry in $\text{Li}_2\text{Pt}_3\text{B}$, *Phys. Rev. Lett.* **98**, 047002 (2007).
- [5] J. Chen, M. B. Salamon, S. Akutagawa, J. Akimitsu, J. Singleton, J. L. Zhang, L. Jiao, and H. Q. Yuan, Evidence of nodal gap structure in the noncentrosymmetric superconductor Y_2C_3 , *Phys. Rev. B* **83**, 144529 (2011).
- [6] S. Harada, J. J. Zhou, Y. G. Yao, Y. Inada, and G.-q. Zheng, Abrupt enhancement of noncentrosymmetry and appearance of a spin-triplet superconducting state in $\text{Li}_2(\text{Pd}_{1-x}\text{Pt}_x)_3\text{B}$ beyond $x = 0.8$, *Phys. Rev. B* **86**, 220502 (2012).
- [7] M. Sato and Y. Ando, Topological superconductors: a review, *Rep. Prog. Phys.* **80**, 076501 (2017).
- [8] C.-L. Zhang, Z. Yuan, G. Bian, S.-Y. Xu, X. Zhang, M. Z. Hasan, and S. Jia, Superconducting properties in single crystals of the topological nodal semimetal PbTaSe_2 , *Phys. Rev. B* **93**, 054520 (2016).
- [9] J. Wang, X. Xu, N. Zhou, L. Li, X. Cao, J. Yang, Y. Li, C. Cao, J. Dai, J. Zhang, Z. Shi, B. Chen, and Z. Yang, Upward Curvature of the Upper Critical Field and the V-Shaped Pressure Dependence of T_c in the Noncentrosymmetric Superconductor PbTaSe_2 , *J. Supercond. Nov. Magn.* **28**, 3173 (2015).
- [10] M. N. Ali, Q. D. Gibson, T. Klimczuk, and R. J. Cava, Noncentrosymmetric superconductor with a bulk three-dimensional Dirac cone gapped by strong spin-orbit coupling, *Phys. Rev. B* **89**, 020505 (2014).
- [11] M. X. Wang, Y. Xu, L. P. He, J. Zhang, X. C. Hong, P. L. Cai, Z. B. Wang, J. K. Dong, and S. Y. Li, Nodeless superconducting gaps in noncentrosymmetric superconductor PbTaSe_2 with topological bulk nodal lines, *Phys. Rev. B* **93**, 020503 (2016).
- [12] G. M. Pang, M. Smidman, L. X. Zhao, Y. F. Wang, Z. F. Weng, L. Q. Che, Y. Chen, X. Lu, G. F. Chen, and H. Q. Yuan, Nodeless superconductivity in noncentrosymmetric PbTaSe_2 single crystals, *Phys. Rev. B* **93**, 060506 (2016).
- [13] M. N. Wilson, A. M. Hallas, Y. Cai, S. Guo, Z. Gong, R. Sankar, F. C. Chou, Y. J. Uemura, and G. M. Luke, μSR study of the noncentrosymmetric superconductor PbTaSe_2 , *Phys. Rev. B* **95**, 224506 (2017).
- [14] T.-R. Chang, P.-J. Chen, G. Bian, S.-M. Huang, H. Zheng, T. Neupert, R. Sankar, S.-Y. Xu, I. Belopolski, G. Chang, B. Wang, F. Chou, A. Bansil, H.-T. Jeng, H. Lin, and M. Z. Hasan, Topological Dirac surface states and superconducting pairing correlations in PbTaSe_2 , *Phys. Rev. B* **93**, 245130 (2016).
- [15] G. Bian, T.-R. Chang, R. Sankar, S.-Y. Xu, H. Zheng, T. Neupert, C.-K. Chiu, S.-M. Huang, G. Chang, I. Belopolski, *et al.*, Topological nodal-line fermions in spin-orbit metal PbTaSe_2 , *Nat. Commun.* **7**, 1 (2016).
- [16] L. Fu and C. L. Kane, Superconducting Proximity Effect and Majorana Fermions at the Surface of a Topological Insulator, *Phys. Rev. Lett.* **100**, 096407 (2008).
- [17] P.-J. Chen, T.-R. Chang, and H.-T. Jeng, Ab initio study of the PbTaSe_2 -related superconducting topological metals, *Phys. Rev. B* **94**, 165148 (2016).
- [18] O. J. Taylor, A. Carrington, and J. A. Schlueter, Specific-Heat Measurements of the Gap Structure of the Organic Superconductors $\kappa\text{-(ET)}_2\text{Cu}[\text{N}(\text{CN})_2]\text{Br}$ and $\kappa\text{-(ET)}_2\text{Cu}(\text{NCS})_2$, *Phys. Rev. Lett.* **99**, 057001 (2007).
- [19] R. Sankar, G. N. Rao, I. P. Muthuselvam, T.-R. Chang, H. Jeng, G. S. Murugan, W.-L. Lee, and F. Chou, Anisotropic superconducting property studies of single crystal PbTaSe_2 , *J. Phys. Condens. Matter.* **29**, 095601 (2017).

- [20] J. M. Ziman, *Electrons and Phonons* (Oxford University Press, 2001).
- [21] Y.-J. Long, L.-X. Zhao, P.-P. Wang, H.-X. Yang, J.-Q. Li, H. Zi, Z.-A. Ren, C. Ren, and G.-F. Chen, Single crystal growth and physical property characterization of non-centrosymmetric superconductor PbTaSe_2 , *Chin. Phys. Lett.* **33**, 037401 (2016).
- [22] M. Wilson, A. Hallas, Y.-p. Cai, S. Guo, Z. Gong, R. Sankar, F. Chou, Y. Uemura, and G. Luke, μ SR study of the noncentrosymmetric superconductor PbTaSe_2 , *Phys. Rev. B* **95**, 224506 (2017).
- [23] Y. Sun, S. Kittaka, T. Sakakibara, K. Machida, R. Sankar, X. Xu, N. Zhou, X. Xing, Z. Shi, S. Pyon, *et al.*, Fully gapped superconductivity without sign reversal in the topological superconductor PbTaSe_2 , *Phys. Rev. B* **102**, 024517 (2020).
- [24] F. Bouquet, Y. Wang, R. Fisher, D. Hinks, J. Jorgensen, A. Junod, and N. Phillips, Phenomenological two-gap model for the specific heat of MgB_2 , *Europhys. Lett.* **56**, 856 (2001).
- [25] A. Carrington and F. Manzano, Magnetic penetration depth of MgB_2 , *Physica C* **385**, 205 (2003).
- [26] R. Khasanov, A. Shengelaya, A. Maisuradze, D. Di Castro, I. Savić, S. Weyeneth, M. Park, D. Jang, S.-I. Lee, and H. Keller, Nodeless superconductivity in the infinite-layer electron-doped cuprate superconductor $\text{Sr}_{0.9}\text{La}_{0.1}\text{CuO}_2$, *Phys. Rev. B* **77**, 184512 (2008).
- [27] W. L. McMillan, Transition Temperature of Strong-Coupled Superconductors, *Phys. Rev.* **167**, 331 (1968).
- [28] M. Bouvier, P. Lethuillier, and D. Schmitt, Specific heat in some gadolinium compounds. I. Experimental, *Phys. Rev. B* **43**, 13137 (1991).
- [29] J. Henheik, E. Langmann, and A. B. Lauritsen, Multi-band superconductors have enhanced critical temperatures, arXiv:2409.17297.
- [30] J. Yu, C. J. Ciccarino, R. Bianco, I. Errea, P. Narang, and B. A. Bernevig, Non-trivial quantum geometry and the strength of electron-phonon coupling, *Nat. Phys.* **20**, 1262 (2024).